Supplementary Information for

Theoretical modeling of contact-separation mode triboelectric nanogenerators from initial charge distribution

Hongfa Zhao[1,7], Hao Wang[2,7], Hongyong Yu[2], Qinghao Xu[1], Xiaosa Li[1], Jing Guo[1], Jiajia Shao[3], Zhong Lin Wang[3,4,5*], Minyi Xu[2*], Wenbo Ding[1,6*]

[1] Tsinghua-Berkeley Shenzhen Institute, Shenzhen International Graduate School, Tsinghua University, Shenzhen 518055, China.

[2] Marine Engineering College, Dalian Maritime University, Dalian 116026, China.

[3] Beijing Institute of Nanoenergy and Nanosystems, Chinese Academy of Sciences, Beijing 100085, China.

[4] School of Materials Science and Engineering, Georgia Institute of Technology, Atlanta, GA 30332-0245, USA.

[5] Yonsei Frontier Lab, Yonsei University, Seoul 03722, Republic of Korea

[6] RISC-V International Open Source Laboratory, Shenzhen 518055, China.

[7] These authors contributed equally: Hongfa Zhao, Hao Wang

*Email: zhong.wang@mse.gatech.edu; xuminyi@dlmu.edu.cn; dingwenbo@sz.tsinghua.edu.cn

This file includes:

Tables S1-S2

Notes S1-S25

Table S1. Theoretical models proposed in the study.

	Models	Section	Initial source charges	Contents	Application	Assumption	Limitation
1	Basic models for tribo-charge layers	Section 2 Figure 3a	Charge from contact electrification for the first model, and pre-charging charge for the second model	Analysis for charge distribution and electric field distribution	Tribo-charge layers	A dielectric material and an independent electrode, charges are distributed uniformly	Only analysis for basic tribo-charge layers
2	Model for the first type of TENG	Section 3 Figure 3d	Charge from contact electrification	Analytical solution of charge distribution and electric field distribution	First type of TENG	Only consider uniformly distributed triboelectric charges on the dielectric material and independent electrode, surface charges, infinite plate model	Only applied for CS TENG with triboelectric charges
3	Model for the second type of TENG	Section 3 Figure 3g	Pre-charging of dielectric material	Analytical solution of charge distribution and electric field distribution	Second type of TENG	Only consider uniformly distributed pre-charging triboelectric charges on the dielectric material, surface charges, infinite plate model	Only applied for CS TENG with pre-charging triboelectric charges
4	A general TENG model	Section 4 Figure 4a	Charge from contact electrification, pre-charging charge, and compensation charge	Analytical solution of charge distribution, electric field distribution, charge transfer process, output performance of TENGs, and displacement current	General for contact-separation mode TENGs	Consider uniformly distributed triboelectric charges on the dielectric material and independent electrode, pre-charging triboelectric charges on the dielectric material, and compensation charge on the base electrode, surface charges, infinite plate model	Applied for the case the size of the TENG is much larger that its internal distance, providing guidance for TENG in practice, while not 100% accurate due to the estimated error in practice
5	Single-electrode TENG model converting from the	Section 5 Figure 6a	Charge from contact electrification, pre-charging charge	Analytical solution of charge distribution, electric field distribution, charge transfer	Validation approach	Consider all charges in 4, while the charge distribution of the TENG will be changed when one electrode is	Applied for the case when one electrode is grounded

	general TENG model			process, and output performance of TENGs		grounded	
6	Electrodynamic model	Section 6 Figure 9a	Charge from contact electrification, pre-charging charge, compensation charge, and electric dipole. Or surface charge, bulk charge, and electric dipole.	Analysis for charge distribution, electric field distribution, charge transfer process, output performance of TENGs, and displacement current	More precise approach	Consider all charges in 4, while the charges on the dielectric material can be surface charges or bulk charges, and consider electric dipole, finite plate model	More general and accurate than other models, but complex and computationally intensive, only has numerical solution, not intuitive for optimizing TENG in practice

Table S2. Comparison of the typical theoretical models for the CS mode TENG.

Part 1.

References	Year	Contents			Applicable range		
		Infinite plate models	Finite plate models	Comparison of two kinds of models	Dielectric to electrode	Dielectric to dielectric	Different types of TENGs
Reference 1[1]	2013	⚑			⚑	⚑	
Reference 2[2]	2016	⚑			⚑		
Reference 3[3]	2017		⚑			⚑	
Reference 4[4]	2017		⚑			⚑	
Reference 5[5]	2023		⚑		⚑		
This study	Now	⚑	⚑	⚑	⚑	⚑	⚑

Part 2.

References	Initial charge distribution			Self-consistency, mechanism for charge redistribution			
	Triboelectric charges	Pre-charging charges	Compensation charges	Charge redistribution on electrodes	Charge convention	Zero electric field of electrodes	Equal potential of connected electrodes
Reference 1	⚑						
Reference 2	⚑				⚑		
Reference 3	⚑						⚑
Reference 4	⚑						
Reference 5	⚑						
This study	⚑	⚑	⚑	⚑	⚑	⚑	⚑

Part 3.

References	Details for derivations						
	Intuitive analytical solutions	Nonintuitive analytical solutions	Numerical solutions	Details for simulations	Comparison of those solutions	Detailed mechanism for equations	Step by step derivations
Reference 1	⚑	⚑	⚑				
Reference 2		⚑	⚑				
Reference 3		⚑	⚑				
Reference 4		⚑	⚑				
Reference 5			⚑				
This study	⚑		⚑	⚑	⚑	⚑	⚑

Part 4.

References	Validation approaches		Application in practice	
	Estimated parameters substitution	New and more rigorous validation approaches	Explanation for exited experimental phenomena	Extension analysis for other applications
Reference 1	⚑			
Reference 2	⚑			
Reference 3	⚑			
Reference 4	⚑			
Reference 5	⚑			
This study	⚑	⚑	⚑	⚑

Note S1 Detailed explanation for the electrostatic equilibrium states of electrode and dielectric materials.

Fig. 1b is a schematic diagram to qualitatively describe the complex charge distribution of TENGs before we introduce the analytical approaches. It demonstrates some points of view: 1. For the conductor-to-dielectric CS mode TENG, the dielectric material (like FEP) we used usually has a strong electronegativity. Before the TENG is made, the dielectric material may have acquired negative charges from the contact electrification process with other materials in the environment. In addition, it's also not uncommon to pre-charge the dielectric material via contact electrification, as the TENG is fabricated. For these reasons, as of the whole TENG, the negative charges usually exceed positive charges. 2. After the TENG is ready, the dielectric material and the independent electrode contact and separate, so the independent electrode gets positive charges, and the dielectric material gets additional negative charges. Therefore, when the electrodes are connected, the electrodes have net positive charges. 3. Under the influence of the negative charges, the electrodes separate positive and negative charges to reach their electrostatic equilibrium states. The internal electric field intensities of the electrodes should be zero. So the positive and negative charges coexist at the same time.

We can use an example to explain this. As shown in Fig. N1, the schematic diagrams of the electrode and dielectric material is shown in Fig. N1i and Fig. N1ii. When the two materials are combined (Fig. N1ii), under the influence of the negative charges, the electrode separates positive and negative charges to reach electrostatic equilibrium state. As the dielectric material is removed (Fig. N1iv), the positive and negative charges in the electrode will recombine and the electrode return to its initial state. If the two materials contact and separate, the electrode will have additional positive charges due to contact electrification. In this case, the electrode will have both positive and negative charges, and negative charges exceed positive charges.

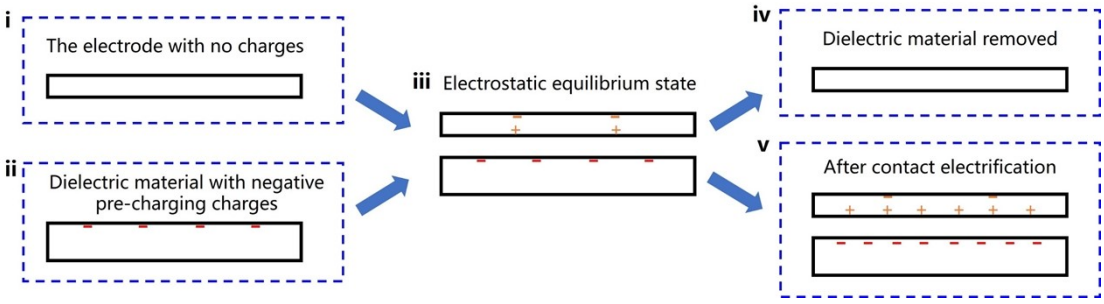

Fig. N1 Schematic diagrams for charge distributions of two materials under different states.

Note S2. Simulations for the potential and electric field of the tribo-charge layers after CE.

In the simulation, the infinite plate model is utilized. The upper plate is an independent electrode set as aluminum material, while the lower plate is a dielectric material set as Polytetrafluoroethylene (PTFE) material in the model. The potential of the model at lower infinity is specified as 0. In the electric field diagram (Fig. 3b, Fig. N2a), the electric field is confined to the region between the two plates, with zero electric field present elsewhere. In the potential distribution diagram (Fig. N2b-c), increasing potential only exists between the two plates, with zero potential in the lower region and an equivalent value (to that of the independent electrode) in the upper region (no variation within areas where electric field intensity is zero).

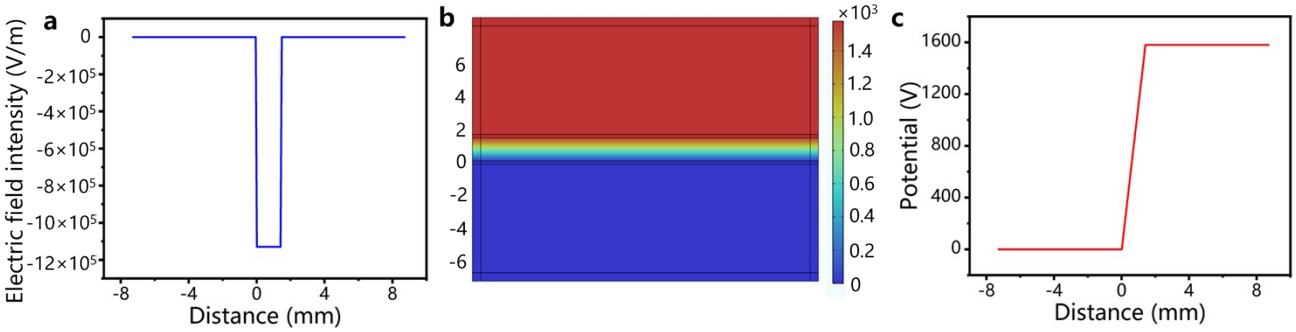

Fig. N2 Simulation results of the potential and electric field. **a** Variation of the electric field intensity with the distance. **b** Distribution of the potential. **c** Variation of the potential with the distance. At the upper surface of the dielectric material distance = 0.

Note S3. Theoretical analysis for the single-electrode TENG model.

When a conductor is grounded, its potential becomes zero (Fig. N3). The internal field intensity of the conductor is zero and there is no electric field above it (the potential at infinity is also zero). In this case, obviously, the potential at the surface of the dielectric material is Ez_0. Compared with the model depicted in Fig. 3a, there is no change in charge distribution, because the electric field inside the conductor is zero as equilibrium has been reached in the beginning.

Simulation results are consistent with the analytical solution. The distribution of the electric field is the same in the two models (Fig. N4a-b). As for the distribution of the potential, the absolute value of the potential changes but the relative value remains the same (Fig. N4c-d). Even after increasing the distance between the dielectric material and the independent electrode, the uniform electric field is still confined to specific region where the potential increases proportionally (Fig. N5). Especially in the infinite plate model, the induced charge density σ is determined by the charge density $-\sigma_t$ on the dielectric material and is independent of the distance z_0 between the two materials. This result indicates that variations in the distance z_0 do not lead to charge transfer or varying voltage across the resistance. But if the electric field between the two materials is not uniform, the charge on the conductor will be distance-dependent and there will a voltage and current change through the resistance. Therefore, an electrodynamic model should be adopted to calculate the output performance of a single-electrode TENG[6-8].

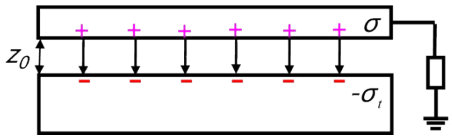

Fig. N3 Schematic diagram of charge distribution of the single-electrode TENG.

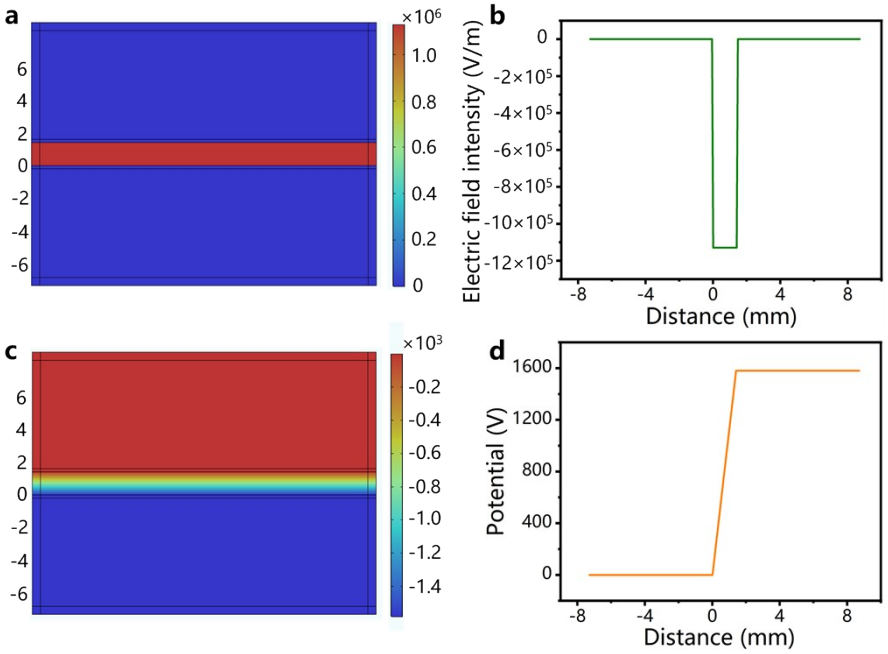

Fig. N4 Simulation results of the single-electrode TENG model with the independent electrode grounded. **a** Distribution of the electric field. **b** Variation of the electric field intensity with the distance. **c** Distribution of the potential. **d** Variation of the potential with the distance.

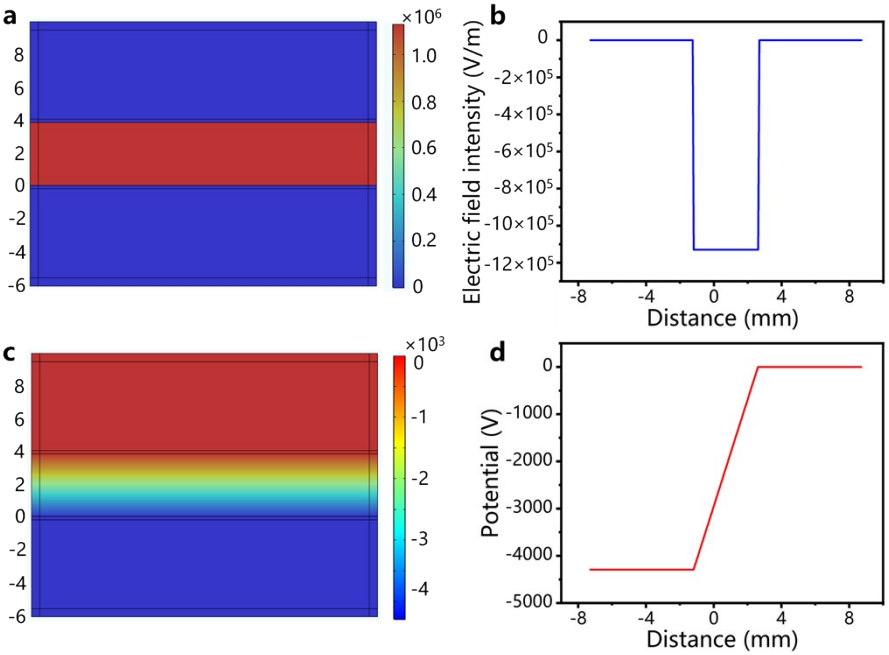

Fig. N5 Simulation results of the single-electrode TENG model with a larger internal distance. **a** Distribution of the electric field **b** Variation of the electric field intensity with the distance. **c** Distribution of the potential. **d** Variation of the potential with the distance.

Note S4. Analysis of the charge distribution and electric field with a pre-charging dielectric material.

When the dielectric material is pre-charged by CE (with external materials), the distribution diagram of the electric field and the corresponding simulation result are shown in Fig. N6ai and N6b. When the independent electrode is added into the system, the total electric field at any given point A inside the electrode should be zero. By solving the equations:

$$\begin{cases} -\frac{\sigma_t}{2\varepsilon_0}+\frac{\sigma_1}{2\varepsilon_0}+\frac{\sigma_2}{2\varepsilon_0}=0 \\ \sigma_1-\sigma_2=0 \end{cases}$$

We have:

$$\sigma_1=\sigma_2=\frac{\sigma_t}{2}$$

The upper surface of the electrode has $\sigma_t/2$ negative charges while the bottom surface has equivalent positive charges. Except for the region inside the electrode, the electric field intensity in the other regions remains the same as before. When the electrode is grounded and a resistance is connected in the external circuit, induced charges will appear at the lower surface of the electrode and the charge distribution will be the same as the model in Fig. N3.

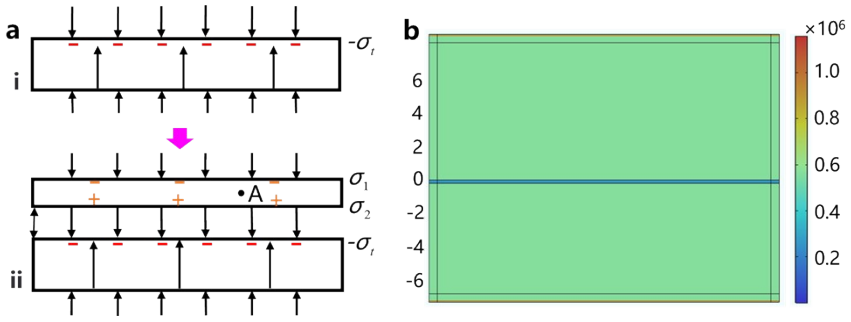

Fig. N6 The distribution of charge and electric field with a pre-charging dielectric material. **a** Schematic diagram of the model. **b** Simulation of the electric field distribution with a pre-charging dielectric material.

Note S5. Open-circuit model corresponding to the first type of tribo-charge layers.

For the open-circuit (contact-separation) TENG model, the base electrode of the dielectric material is introduced to the system (Fig. N7a). Corresponding to the first type of tribo-charge layers, since the electric field is distributed only between the two layers and there is no electric field in the outer space, no induced charge appears at the base electrode and the system remains in the original electrostatic equilibrium. The potential at the upper surface of the dielectric material can be set as zero, then the potential at the upper electrode surface is $\sigma_t z_0 / \varepsilon_0$. Since there are no electric field between the upper surface of the dielectric material and the base electrode, the potential of the base electrode is also zero. The simulation results are consistent with the theoretical analysis (Fig. N7b-c). Compared with the results presented in Note S2, though the base electrode is introduced, the charge and electric field distribution remain the same. Obviously, the potential difference between the two electrodes is still $\sigma_t z_0 / \varepsilon_0$. This voltage is also the potential relative to ground, and the voltage increases with the distance between the two tribo-charge layers.

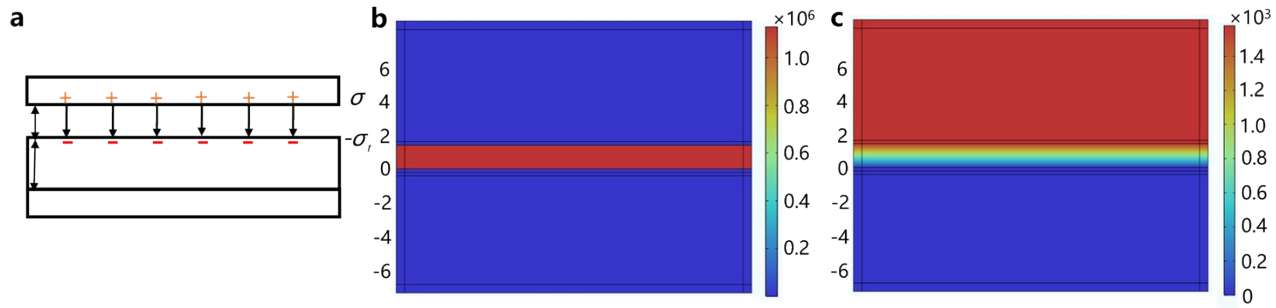

Fig. N7 The open-circuit model and simulation results. **a** Schematic diagram of the model. **b** Distribution of the electric field. **c** Distribution of the potential.

Note S6. Comparison of the potential distribution from analytical solution and simulation results.

Distribution of the potential can be calculated from the electric fields:

$$V_1 = V_4 = 0$$

$$V_2 = -E_2(z - z_b)$$

$$V_3 = E_3(z - z_u)$$

Where V_1, V_2, V_3, V_4 are the potential in different regions, respectively. z_u and z_b is the z coordinates of the upper and bottom surface of the dielectric material, respectively. For the simulation results, the potential of the independent electrode and the base electrode are equivalent (Fig. N8). The electric field intensity inside the two electrodes is zero, and the potential distribution from simulation is consistent with that derived analytically, thus validating its accuracy.

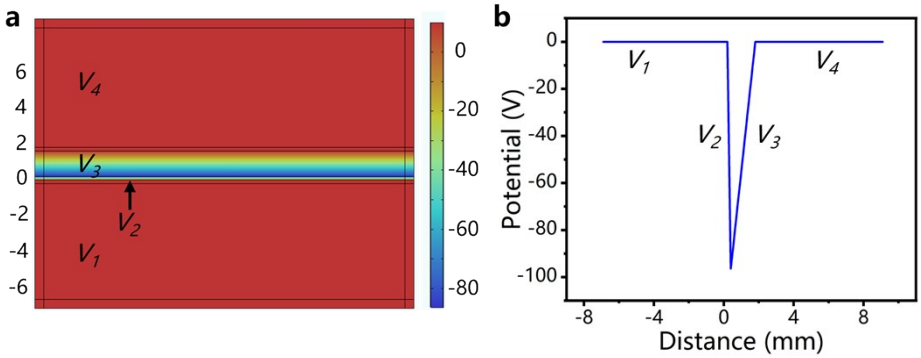

Fig. N8 Simulation results of the potential. **a** Distribution of the potential. **b** Variation of the potential with the distance.

Note S7. Open-circuit model corresponding to the second type of tribo-charge layers.

In the open circuit state, both electrodes reach electrostatic equilibrium (Fig. N9a). At any given point A and B inside the electrodes, the electric field intensity is zero. Based on conservation of charge, the following equations can be achieved:

$$\begin{cases} -\sigma_1 + \sigma_2 = 0 \\ \sigma_3 - \sigma_4 = 0 \\ -\dfrac{\sigma_t}{2\varepsilon_0} + \dfrac{\sigma_1}{2\varepsilon_0} + \dfrac{\sigma_2}{2\varepsilon_0} + \dfrac{\sigma_3}{2\varepsilon_0} - \dfrac{\sigma_4}{2\varepsilon_0} = 0 \\ \dfrac{\sigma_t}{2\varepsilon_0} + \dfrac{\sigma_1}{2\varepsilon_0} - \dfrac{\sigma_2}{2\varepsilon_0} - \dfrac{\sigma_3}{2\varepsilon_0} - \dfrac{\sigma_4}{2\varepsilon_0} = 0 \end{cases}$$

The solution is:

$$\sigma_1 = \sigma_2 = \sigma_3 = \sigma_4 = \frac{\sigma_t}{2}$$

The distribution of the electric field in the space is:

$$\mathbf{E_1} = \frac{\sigma_t}{2\varepsilon_0}\mathbf{e_z}$$

$$\mathbf{E_2} = \frac{\sigma_t}{2\varepsilon_0\varepsilon_r}\mathbf{e_z}$$

$$\mathbf{E_3} = -\frac{\sigma_t}{2\varepsilon_0}\mathbf{e_z}$$

$$\mathbf{E_4} = -\frac{\sigma_t}{2\varepsilon_0}\mathbf{e_z}$$

Assuming that z_0 = 1.4 mm, d_0 = 0.2 mm, $\sigma_t = 10^{-5}$ C/m^2, $\varepsilon_r = 2.2$ (as mentioned in the manuscript), the charge distribution can be calculated easily and then these parameters (including the charge on electrodes) are input into the finite element simulation. The simulated distribution of electric field is consistent with that derived theoretically (Fig. N9b-c). Additionally, the potential difference between the two electrodes can be calculated as:

$$\begin{aligned} V &= E_2 d_0 + E_3 z_0 \\ &= \left(\frac{\sigma_t}{2\varepsilon_0\varepsilon_r} + \frac{\sigma_1}{2\varepsilon_0\varepsilon_r} - \frac{\sigma_2}{2\varepsilon_0\varepsilon_r} + \frac{\sigma_3}{2\varepsilon_0\varepsilon_r} - \frac{\sigma_4}{2\varepsilon_0\varepsilon_r} \right) d_0 + \left(-\frac{\sigma_t}{2\varepsilon_0} + \frac{\sigma_1}{2\varepsilon_0} - \frac{\sigma_2}{2\varepsilon_0} + \frac{\sigma_3}{2\varepsilon_0} - \frac{\sigma_4}{2\varepsilon_0} \right) z_0 \\ &= \frac{\sigma_t d_0 - \varepsilon_r \sigma_t z_0}{2\varepsilon_0\varepsilon_r} \end{aligned}$$

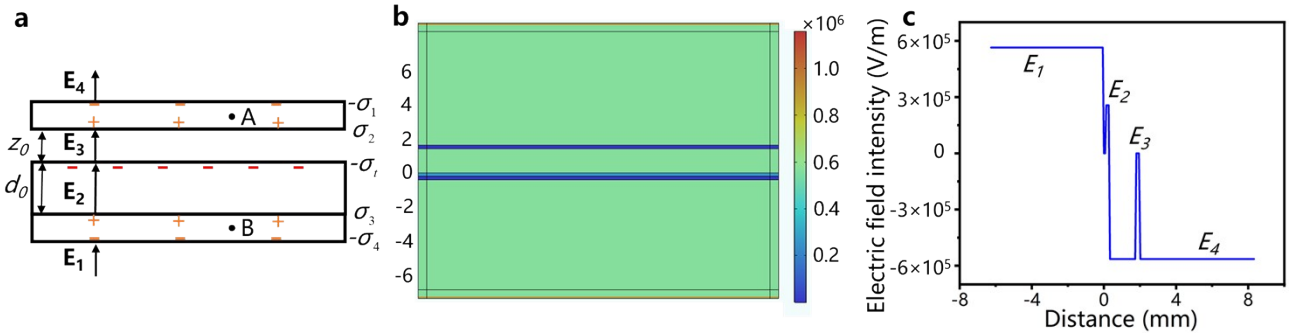

Fig. N9 The open-circuit model and simulation results for electric field distribution. **a** Schematic diagram of the model. **b** Distribution of the electric field. **c** Variation of the electric field intensity with the distance.

Note S8. Analysis of the general open-circuit model.

The open-circuit model is shown in Fig. 4aii. To fulfill charge conservation and electrostatic equilibrium of the electrodes, the following equations can be derived:

$$\begin{cases} -\sigma_1 + \sigma_2 = 0 \\ \sigma_3 - \sigma_4 = 0 \\ -\dfrac{\sigma_t + \sigma_t'}{2\varepsilon_0} + \dfrac{\sigma_1}{2\varepsilon_0} + \dfrac{\sigma_2 + \sigma_2'}{2\varepsilon_0} + \dfrac{\sigma_3 + \sigma_c}{2\varepsilon_0} - \dfrac{\sigma_4}{2\varepsilon_0} = 0 \\ \dfrac{\sigma_t + \sigma_t'}{2\varepsilon_0} + \dfrac{\sigma_1}{2\varepsilon_0} - \dfrac{\sigma_2 + \sigma_2'}{2\varepsilon_0} - \dfrac{\sigma_3 + \sigma_c}{2\varepsilon_0} - \dfrac{\sigma_4}{2\varepsilon_0} = 0 \end{cases}$$

The solution is:

$$\sigma_1 = \sigma_2 = \sigma_3 = \sigma_4 = \frac{\sigma_t - \sigma_c}{2}$$

Therefore, the charges on both (upper and lower) surfaces of each electrode are $-\dfrac{\sigma_t - \sigma_c}{2}$, $\dfrac{\sigma_t - \sigma_c + 2\sigma_t'}{2}$, $\dfrac{\sigma_t + \sigma_c}{2}$, $-\dfrac{\sigma_t - \sigma_c}{2}$, respectively. The potential difference between the two electrodes is:

$$\begin{aligned} V &= E_2 d_0 + E_3 z_0 \\ &= \left(\frac{\sigma_t + \sigma_t'}{2\varepsilon_0\varepsilon_r} + \frac{\sigma_1}{2\varepsilon_0\varepsilon_r} - \frac{\sigma_2 + \sigma_t'}{2\varepsilon_0\varepsilon_r} + \frac{\sigma_3 + \sigma_c}{2\varepsilon_0\varepsilon_r} - \frac{\sigma_4}{2\varepsilon_0\varepsilon_r} \right) d_0 + \left(-\frac{\sigma_t + \sigma_t'}{2\varepsilon_0} + \frac{\sigma_1}{2\varepsilon_0} - \frac{\sigma_2 + \sigma_t'}{2\varepsilon_0} + \frac{\sigma_3 + \sigma_c}{2\varepsilon_0} - \frac{\sigma_4}{2\varepsilon_0} \right) z_0 \\ &= \left(\frac{\sigma_t + \sigma_t'}{2\varepsilon_0\varepsilon_r} + \frac{\sigma_t - \sigma_c}{4\varepsilon_0\varepsilon_r} - \frac{\sigma_t - \sigma_c + 2\sigma_2'}{4\varepsilon_0\varepsilon_r} + \frac{\sigma_t + \sigma_c}{4\varepsilon_0\varepsilon_r} - \frac{\sigma_t - \sigma_c}{4\varepsilon_0\varepsilon_r} \right) d_0 \\ &+ \left(-\frac{\sigma_t + \sigma_t'}{2\varepsilon_0} + \frac{\sigma_t - \sigma_c}{4\varepsilon_0} - \frac{\sigma_t - \sigma_c + 2\sigma_t'}{4\varepsilon_0} + \frac{\sigma_t + \sigma_c}{4\varepsilon_0} - \frac{\sigma_t - \sigma_c}{4\varepsilon_0} \right) z_0 \\ &= \frac{(\sigma_t + \sigma_c) d_0 + (\sigma_t - \sigma_c + 2\sigma_t') \varepsilon_r z_0}{2\varepsilon_0\varepsilon_r} \end{aligned}$$

Assuming that z_0 = 1.4 mm, d_0 = 0.2 mm, $\sigma_t = 6\times10^{-6}$ C/m^2, $\sigma_t' = 4\times10^{-6}$ C/m^2, $\sigma_c = 2\times10^{-6}$ C/m^2, $\varepsilon_r = 2.2$, thus the charge distribution can be deduced and further the electric field:

$$E_1 = \frac{\sigma_t - \sigma_c}{2\varepsilon_0} = \frac{4\times10^{-6}}{2\varepsilon_0}\ \text{V/m} = 2.26\times10^5\ \text{V/m}$$

$$E_2 = \frac{\sigma_t + \sigma_c}{2\varepsilon_0\varepsilon_r} = \frac{8\times10^{-6}}{2\varepsilon_0\varepsilon_r}\ \text{V/m} = 2.05\times10^5\ \text{V/m}$$

$$E_3 = -\frac{\sigma_t - \sigma_c + 2\sigma_t'}{2\varepsilon_0} = -\frac{1.2\times10^{-5}}{2\varepsilon_0}\ \mathrm{V/m} = -6.78\times10^{5}\ \mathrm{V/m}$$

$$E_4 = -\frac{\sigma_t - \sigma_c}{2\varepsilon_0} = -\frac{4\times10^{-6}}{2\varepsilon_0}\ \mathrm{V/m} = -2.26\times10^{5}\ \mathrm{V/m}$$

And then these parameters (including the charge on electrodes) are input into the finite element simulation to get the distribution of electric field. The results are shown in Fig. 4b-c, which are consistent with the calculations, indicating that the solutions above are accurate.

Note S9. Analysis for the charge transfer process of the TENG.

The reference[9] introduces that charges on the dielectric material and the metal electrode have forward-flow and backflow process in the contact electrification process, and finally achieve a stable state. Studies for TENG consider the output performance in both the unstable state and the stable state, but usually the output performance in the stable state is focused.

In this study, considering the backflow phenomenon, it can have influence on the initial charge distribution (triboelectric charges) for the TENG model, which can be explained by the general model. We have given the charge distribution, transferred charge, and current of the TENG in the manuscript:

$$\begin{cases} \sigma_1 = \dfrac{\sigma_t - \sigma_c}{2} \\ \sigma_2 = \dfrac{(\sigma_t + \sigma_t')d_0}{z_0\varepsilon_r + d_0} \\ \sigma_3 = \dfrac{(\sigma_t + \sigma_t')z_0\varepsilon_r}{z_0\varepsilon_r + d_0} \\ \sigma_4 = \dfrac{\sigma_t - \sigma_c}{2} \end{cases} \tag{16}$$

$$Q = \int_{z_1}^{z_2} dQ = \int_{z_1}^{z_2} \frac{(\sigma_t + \sigma_t')\varepsilon_r S d_0}{(z\varepsilon_r + d_0)^2} dz = (\sigma_t + \sigma_t')\varepsilon_r S d_0 \int_{z_1}^{z_2} \frac{dz}{(z\varepsilon_r + d_0)^2} = \frac{(\sigma_t + \sigma_t')\varepsilon_r S d_0 (z_2 - z_1)}{(z_1\varepsilon_r + d_0)(z_2\varepsilon_r + d_0)} \tag{24}$$

$$I(t) = \frac{dQ}{dt} = \frac{dQ}{dz}v = \frac{(\sigma_t + \sigma_t')\varepsilon_r S d_0 v}{(z\varepsilon_r + d_0)^2} \tag{25}$$

In these equations, σ_t' represents the charge density for triboelectric charges. The forward-flow and backflow process of the charges between the dielectric material and electrode will increase or decrease the value for this parameter. Therefore, the output performance of the TENG can still be analyzed by the equations.

To explain the charge transfer process more clearly, We analyze the charge distribution and charge transfer combining with the schematic diagram and equations. As shown in Fig. N10, when the TENG come into contact, corresponding to the process of Fig. N10i to Fig. N10ii, the internal distance z of the TENG decreases. According to eqn (16), σ_2 will increase while σ_3 will decrease, a negative value will be achieved from eqn (24). That means charge transfer from the base electrode of the dielectric material to the independent electrode. While when the TENG is in the separation process, corresponding to the process of Fig. N10ii to Fig. N10iii, the internal distance z of the TENG increases.

According to eqn (16), σ_2 will decrease while σ_3 will increase, a positive value will be achieved from eqn (24). That means charge transfer from the independent electrode to the base electrode of the dielectric material, which is the backflow process. For the current equation, the velocity v has its direction, and the direction of the current is determined by the direction of the velocity.

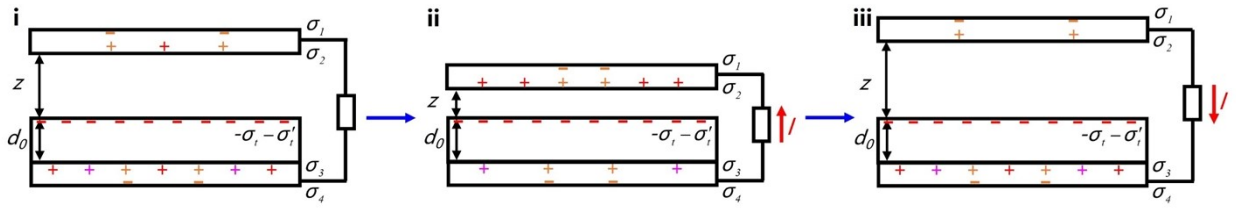

Fig. N10 Schematic diagram for the charge transfer process of the TENG.

Note S10. Estimated parameters for the TENG.

A set of reasonable parameters defining charge distribution and motion states is input into the theoretical model. It is assumed that $d_0 = 0.05$ mm, $\sigma_t = 5\times10^{-4}$ C/m^2, $\sigma_c = 4.72\times10^{-4}$ C/m^2, $\varepsilon_r = 2.2$. Other parameters of charge distribution can be calculated as $\sigma_1 = 1.4\times10^{-5}$ C/m^2, $\sigma_2 = 1.4\times10^{-5}$ C/m^2, $\sigma_3 = 4.86\times10^{-4}$ C/m^2, $\sigma_4 = 1.4\times10^{-5}$ C/m^2, and further, $E_3 = 1.58\times10^{6}$ V/m. It is assumed that the dielectric film of the TENG undergoes sinusoidal motion under the excitation of acoustic waves, $z = 3\times10^{-5}\sin160\pi t + 1\times10^{-4}$, and under an estimated effective working area of about 9 cm^2. The output performance of the TENG can be calculated based on these conditions. It should be noted that open-circuit voltage and transferred charge can be influenced by baseline drifting in experimental measurements, while we usually focus on their peak-to-peak values[10, 11]. In contrast, the current is less affected by the baseline drifting and its value fluctuates above and below the zero line due to alternating positive and negative velocities[12, 13].

Note S11. Experimental data for the acoustic-driven TENG.

The acoustic-driven TENG can convert sound waves into electrical outputs, which is introduced in our previous study[14]. The open-circuit, shot-circuit current and transferred charge are shown in Fig. N11. It should be noted that it's the same experiment with Fig. 6g-i in the manuscript. The comparison of the values and waveforms (between the experimental data and analytical results) indicates that the analytical solution is accurate. The voltage, current and transferred charge are measured separately in the experiment, and the phase difference between them cannot be shown in the experimental data, but it is reflected analytically, which is also the advantage of the theoretical analysis.

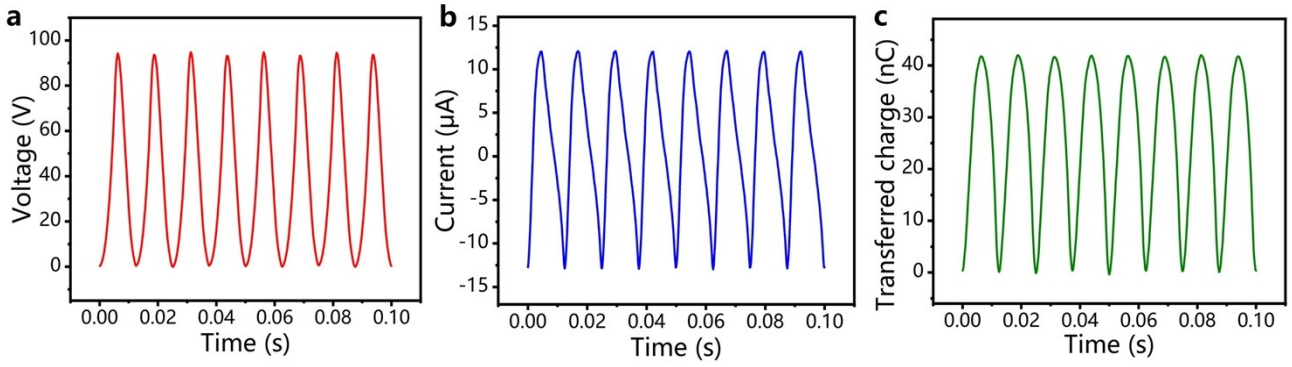

Fig. N11 Output performance of the acoustic-driven TENG. **a** Open-circuit voltage **b** short-circuit current and **c** transferred charge of the acoustic-driven TENG.

Note S12. Analysis for dielectric-to-dielectric CS mode TENGs.

We appreciate the insightful comment from the reviewer. Conductor-to-dielectric CS mode TENGs and dielectric-to-dielectric CS mode TENGs are all important types of TENGs. In fact, the analytical approaches proposed in this study can also be used to analyze dielectric-to-dielectric CS mode TENGs. Comparing these two types of TENGs, conductor-to-dielectric CS mode TENGs are relatively more typical and commonly utilized, actually there are so many interesting studies on this type of TENGs (*Science, 2019, 365 (6452): 491-494*; *Science Robotics, 2018, 3 (20): eaat2516*; *Nature communications, 11 (1), 2020: 5381*), so we choose to analyze this type of TENGs at first. But we can also analyze the dielectric-to-dielectric CS mode TENGs systematically in the future work (the modelling process is largely similar). The following is an analysis for the open-circuit model.

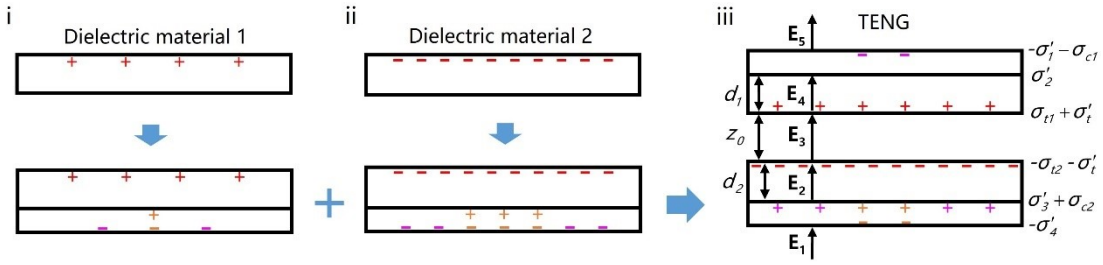

Fig. N12 Theoretical model for the dielectric-to-dielectric CS mode TENG.

A theoretical model for the dielectric-to-dielectric CS mode TENG is shown in Fig. N12. We have the dielectric material 1 on the upper side and the dielectric material 2 on the lower side. The dielectric material 1 maybe have positive pre-charging charges σ_{t1} (red color), the negative compensation charges acquired by the top electrode σ_{c1} (purple color), and the contact-electrification charges σ_t' (red color). While the dielectric material 2 maybe have negative pre-charging charges σ_{t2} (red color), the positive compensation charges acquired by the bottom electrode σ_{c2} (purple color), and the contact-electrification charges σ_t' (red color). The electrodes will separate some positive and negative charges σ_1', σ_2', σ_3', σ_4' (orange color) to reach electrostatic equilibrium states. To fulfill charge conservation and electrostatic equilibrium, a set of equations can be derived:

$$\begin{cases} \sigma_1 - \sigma_2 = 0 \\ \sigma_3 - \sigma_4 = 0 \\ \dfrac{\sigma_1 + \sigma_{c1}}{2\varepsilon_0} + \dfrac{\sigma_2}{2\varepsilon_0} + \dfrac{\sigma_{t1} + \sigma_t'}{2\varepsilon_0} - \dfrac{\sigma_{t2} + \sigma_t'}{2\varepsilon_0} + \dfrac{\sigma_3 + \sigma_{c2}}{2\varepsilon_0} - \dfrac{\sigma_4}{2\varepsilon_0} = 0 \\ \dfrac{\sigma_1 + \sigma_{c1}}{2\varepsilon_0} - \dfrac{\sigma_2}{2\varepsilon_0} - \dfrac{\sigma_{t1} + \sigma_t'}{2\varepsilon_0} + \dfrac{\sigma_{t2} + \sigma_t'}{2\varepsilon_0} - \dfrac{\sigma_3 + \sigma_{c2}}{2\varepsilon_0} - \dfrac{\sigma_4}{2\varepsilon_0} = 0 \end{cases}$$

The solution is:

$$\begin{cases} \sigma_1' = \sigma_2' = \dfrac{-\sigma_{c1} - \sigma_{t1} + \sigma_{t2} - \sigma_{c2}}{2} \\ \sigma_3' = \sigma_4' = \dfrac{\sigma_{c1} - \sigma_{t1} + \sigma_{t2} - \sigma_{c2}}{2} \end{cases}$$

Therefore, the charges on both (upper and lower) surfaces of each electrode are $\dfrac{\sigma_{c1} + \sigma_{t1} - \sigma_{t2} + \sigma_{c2}}{2}$, $\dfrac{-\sigma_{c1} - \sigma_{t1} + \sigma_{t2} - \sigma_{c2}}{2}$, $\dfrac{\sigma_{c1} - \sigma_{t1} + \sigma_{t2} + \sigma_{c2}}{2}$, $\dfrac{-\sigma_{c1} + \sigma_{t1} - \sigma_{t2} + \sigma_{c2}}{2}$, respectively. The potential difference between the two electrodes is:

$$\begin{aligned} V &= E_2 d_2 + E_3 z_0 + E_4 d_1 \\ &= \frac{(\sigma_3' + \sigma_{c2}) d_2}{\varepsilon_0 \varepsilon_{r2}} + \left(\frac{\sigma_1 + \sigma_{c1}}{2\varepsilon_0} - \frac{\sigma_2'}{2\varepsilon_0} - \frac{\sigma_{t1} + \sigma_t'}{2\varepsilon_0} - \frac{\sigma_{t2} + \sigma_t'}{2\varepsilon_0} + \frac{\sigma_3' + \sigma_{c2}}{2\varepsilon_0} - \frac{\sigma_4'}{2\varepsilon_0}\right) z_0 - \frac{\sigma_2' d_1}{\varepsilon_0 \varepsilon_{r1}} \\ &= \frac{(\sigma_{c1} - \sigma_{t1} + \sigma_{t2} + \sigma_{c2}) d_2}{2\varepsilon_0 \varepsilon_{r2}} + \frac{(2\sigma_{c1} + \sigma_{c2} - \sigma_{t1} - \sigma_{t2} - 2\sigma_t') z_0}{2\varepsilon_0} + \frac{(\sigma_{c1} + \sigma_{t1} - \sigma_{t2} + \sigma_{c2}) d_1}{2\varepsilon_0 \varepsilon_{r1}} \\ &= \frac{(\sigma_{c1} - \sigma_{t1} + \sigma_{t2} + \sigma_{c2}) d_2 \varepsilon_{r1} + (2\sigma_{c1} + \sigma_{c2} - \sigma_{t1} - \sigma_{t2} - 2\sigma_t') z_0 \varepsilon_{r1} \varepsilon_{r2} + (\sigma_{c1} + \sigma_{t1} - \sigma_{t2} + \sigma_{c2}) d_1 \varepsilon_{r2}}{2\varepsilon_0 \varepsilon_{r1} \varepsilon_{r2}} \end{aligned}$$

The schematic diagram in Fig. N12 shows the case when the dielectric 2 material has more negative charges. And another model when the dielectric 1 material has more positive charges is shown in Fig. N13. The proposed approach can also be used to analyze the dielectric-to-dielectric CS mode TENG.

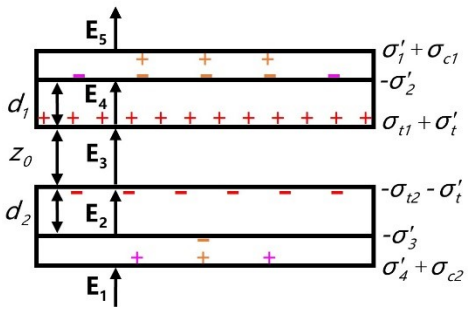

Fig. N13 Another model for the dielectric-to-dielectric CS mode TENG when the dielectric 1 material has more positive charges.

Note S13. Distribution of the electric field for the single-electrode TENG.

Based on the charge distribution, the distribution of the electric is:

$$\mathbf{E_1} = 0$$

$$\mathbf{E_2} = \frac{(\sigma_t + \sigma_t')z_0}{\varepsilon_0\left(z_0\varepsilon_r + d_0\right)}\mathbf{e_z}$$

$$\mathbf{E_3} = -\frac{(\sigma_t + \sigma_t')d_0}{\varepsilon_0\left(z_0\varepsilon_r + d_0\right)}\mathbf{e_z}$$

$$\mathbf{E_4} = 0$$

Obviously, the electric fields $\mathbf{E_2}$ and $\mathbf{E_3}$ inside the TENG are as same as the results calculated for Fig. 4aiii.

Note S14. Theoretical analysis and experimental results for the single-electrode TENG with an electrode suspended.

Usually, the output performance of a single-electrode TENG is much smaller than that of a contact-separation mode TENG of the same size. The schematic diagram of the single-electrode TENG model is shown in Fig. N14a. At any given point A and B inside the electrodes, the electric field intensity is zero, and the potential of the grounded electrode equal to zero, thus a system of equations can be derived:

$$\begin{cases} -\dfrac{\sigma_t+\sigma_t'}{2\varepsilon_0}+\dfrac{\sigma_2}{2\varepsilon_0}+\dfrac{\sigma_3+\sigma_c}{2\varepsilon_0}-\dfrac{\sigma_4}{2\varepsilon_0}=0 \\ \dfrac{\sigma_t+\sigma_t'}{2\varepsilon_0}-\dfrac{\sigma_2}{2\varepsilon_0}-\dfrac{\sigma_3+\sigma_c}{2\varepsilon_0}-\dfrac{\sigma_4}{2\varepsilon_0}=0 \\ \sigma_3-\sigma_4=0 \end{cases}$$

The solution is:

$$\begin{cases} \sigma_2=\sigma_t+\sigma_t'-\sigma_c \\ \sigma_3=\sigma_4=0 \end{cases}$$

It can be seen that the charge distribution on the electrode does not change with the internal distance of the TENG. when the TENG moves under the mechanical excitation to the source, no current flows through the resistance. This analysis is based on the infinite plate model. In the experiment, the current and transferred charge of the single-electrode TENG significantly reduce (Fig. N14b-c). The theoretical analysis could explain the characteristics of the TENG well. But for more accurate results, an electrodynamic model should be utilized.

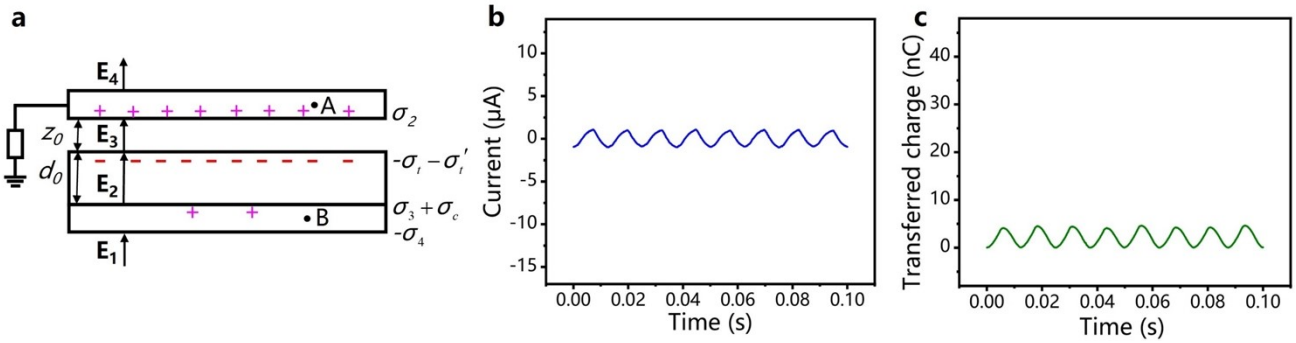

Fig. N14 Theoretical model and experimental results for the single-electrode TENG with an electrode suspended. **a** Schematic diagram of the model. **b** Current and **c** transferred charge of the single-electrode TENG.

Note S15. Theoretical analysis and experimental results for the single-electrode TENG with another electrode grounded.

Different from above, if the base electrode of the dielectric material is used as the outputting electrode (Fig. N15a), to fulfill the electrostatic equilibrium and zero potential of the grounded electrode, a system of equations can be derived:

$$\begin{cases} -\frac{\sigma_t+\sigma_t'}{2\varepsilon_0}+\frac{\sigma_1}{2\varepsilon_0}+\frac{\sigma_2+\sigma_t'}{2\varepsilon_0}+\frac{\sigma_3}{2\varepsilon_0}=0 \\ \frac{\sigma_t+\sigma_t'}{2\varepsilon_0}+\frac{\sigma_1}{2\varepsilon_0}-\frac{\sigma_2+\sigma_t'}{2\varepsilon_0}-\frac{\sigma_3}{2\varepsilon_0}=0 \\ -\sigma_1+\sigma_2=0 \end{cases}$$

The solution is:

$$\begin{cases} \sigma_1=\sigma_2=0 \\ \sigma_3=\sigma_t+\sigma_t'-\sigma_2' \end{cases}$$

Similar to the model in Note S13, the charge distribution on the electrode does not change with the variation of the internal distance of the TENG. The current and transferred charge are shown in Fig. N15b-c, also similar to the experimental results shown in Note S13.

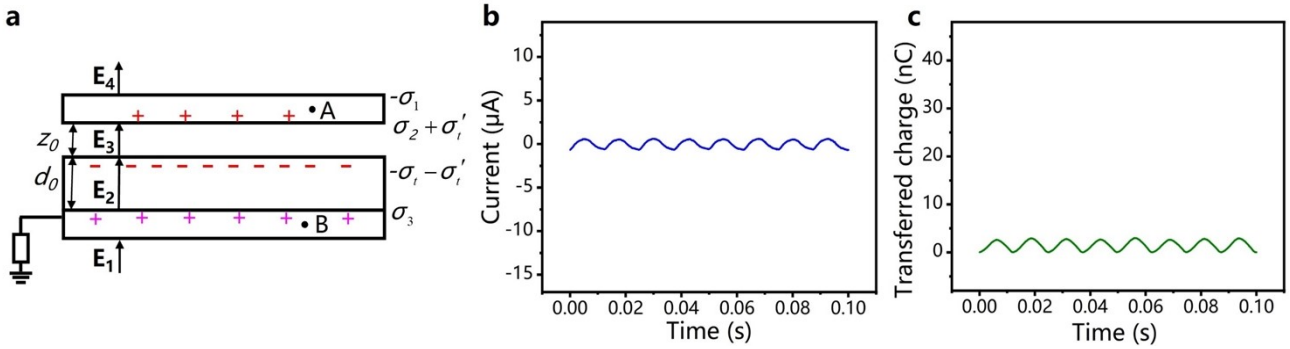

Fig. N15 Theoretical model and experimental results for the single-electrode TENG with the independent electrode suspended. **a** Schematic diagram of the model. **b** Current and **c** transferred charge of the TENG.

When the independent electrode is grounded and the base electrode is utilized as the outputting electrode, the schematic diagram of the model is shown in Fig. N16a. To fulfill the electrostatic

equilibrium and zero potential of the grounded electrode, the equations can be derived:

$$\begin{cases} -\frac{\sigma_t+\sigma_t'}{2\varepsilon_0}+\frac{\sigma_2}{2\varepsilon_0}+\frac{\sigma_3}{2\varepsilon_0}=0 \\ \frac{\sigma_3}{\varepsilon_0\varepsilon_r}d_0-\frac{\sigma_2}{\varepsilon_0}z_0=0 \end{cases}$$

The solution is:

$$\begin{cases} \sigma_2=\frac{(\sigma_t+\sigma_t')d_0}{z_0\varepsilon_r+d_0} \\ \sigma_3=\frac{(\sigma_t+\sigma_t')z_0\varepsilon_r}{z_0\varepsilon_r+d_0} \end{cases}$$

The charge distribution is the same as the results shown in eqn (27) in the manuscript. Therefore, the output performance of this single-electrode TENG will be as same as that of the single-electrode TENG shown in Fig. 6a. The current and transferred charge from experiment (Fig. N16b-c) also coincide with those shown in Fig. 6k-l. It should be noted that the waveforms are inversed due to different outputting electrode.

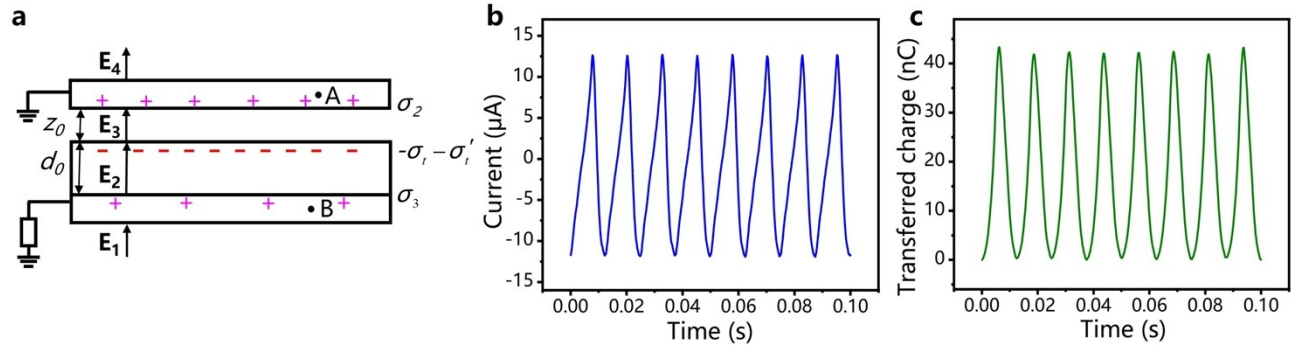

Fig. N16 Theoretical model and experimental results for the single-electrode TENG with the independent electrode grounded. **a** Schematic diagram of the model. **b** Current and **c** transferred charge of the TENG.

Note S16. The grounding method for the transformed SE mode TENG.

In an obvious aspect, the acoustic TENG used in the experiment has an output of 94.5 V, 13 μA, and 42 nC. It's not easy for the SE mode TENG to affect the measurement device and form a circuit loop. And if the current can flow from the ground to the electrometer and then to another electrode of the TENG, there should be a significant part of the current flow into the earth, so that the measured signal should be smaller than the original CS mode TENG. While the output performance of the CS mode TENG is nearly the same as that of the transformed SE mode TENG. Therefore, this characteristic of the TENG is not easy and should be explained by theoretical models and rigorous derivations.

For the grounding methods, as shown in Fig. N17i, one electrode is put onto the ground about 50 meters away from the measurement system, and the other electrode of the TENG is connected to the electrometer. In this case, the electron transfer between the electrode and the ground may not affect the measurement device.

The second method is shown in Fig. N17ii, the TENG is put onto the ground with an insulating box so that the current cannot form a circuit loop. In fact, this is an approximate ground method. When the capacitance (volume) of the ground is much larger than the electrode of the TENG, the TENG is almost grounded, and it is discussed based on derivations in the "practical applications based on the proposed theory" section in the manuscript.

And for the third method shown in Fig. N17iii, we use a current acquisition board to measure the output of the TENG. The data is sent to the computer by an ESP32 board via WiFi. The measurement system is introduced in a previous study[15], and the photos of the current acquisition board and ESP32 board are shown in Fig. N18.

For the three grounding methods, the output performance of the CS mode TENG is nearly the same as that of the transformed SE mode TENG. Therefore, we use theoretical models and physical derivations to explain this characteristic of the TENG.

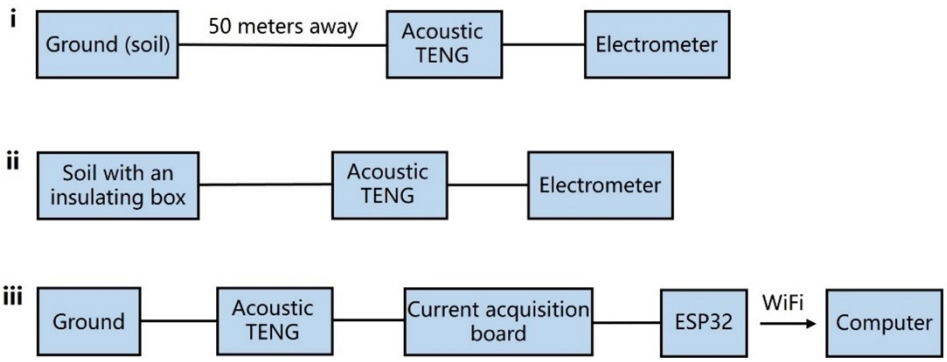

Fig. N17 Grounding method for the transformed SE mode TENG.

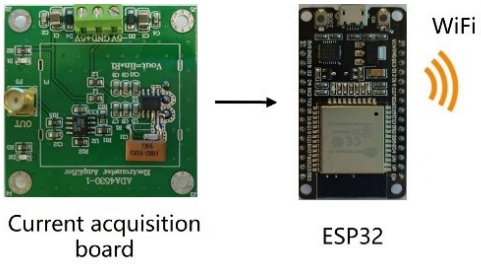

Fig. N18 Photos of the current acquisition board and ESP32 board.

Note S17. Derivation process for the voltage between the two electrodes with a large resistance.

If the two electrodes are connected by a large resistance sufficient to affect the charge transfer process during the change of the internal distance z, when the distance increases by dz, the voltage between the two electrodes increases by:

$$dV' = \frac{(\sigma_t + \sigma_t')d_0 dz}{\varepsilon_0 (z\varepsilon_r + d_0)}$$

The current in the external circuit is:

$$I(t) = \frac{(\sigma_t + \sigma_t')d_0 dz}{\varepsilon_0 (z\varepsilon_r + d_0)R} = \frac{(\sigma_t + \sigma_t')d_0 v dt}{\varepsilon_0 (z\varepsilon_r + d_0)R}$$

And transferred charge is:

$$dQ = \int \frac{(\sigma_t + \sigma_t')d_0 dz dt}{\varepsilon_0 (z\varepsilon_r + d_0)R}$$

When the internal distance increases by another dz, the voltage increases by:

$$dV = \frac{(\sigma_t + \sigma_t')d_0 dz}{\varepsilon_0 (z\varepsilon_r + d_0)} - \frac{2d_0 z}{\varepsilon_0 (z\varepsilon_r + d_0)S} \iint \frac{(\sigma_t + \sigma_t')d_0 v dz dt}{\varepsilon_0 (z\varepsilon_r + d_0)R}$$

So the voltage between the two electrodes is:

$$V = \int \left(\frac{(\sigma_t + \sigma_t')d_0}{\varepsilon_0 (z\varepsilon_r + d_0)} - \frac{2d_0 z}{\varepsilon_0 (z\varepsilon_r + d_0)S} \int \frac{(\sigma_t + \sigma_t')d_0 v dt}{\varepsilon_0 (z\varepsilon_r + d_0)R} \right) dz$$

Note S18. Electric field intensity for infinite plate models.

The electric field intensity for infinite plate models in space is uniformly directed along the *z*-axis (Fig. N19). This is because the charge is distributed on infinite plates, these charges also generate electric fields in transverse direction, and they mutually cancel each other out in space. If the charge is distributed on the finite plates, the electric fields generated by these charges can not fully cancel out each other, so both the magnitude and the direction of the electric field in space are non-uniform.

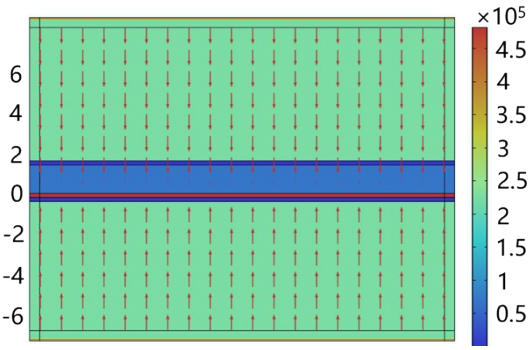

Fig. N19 Electric field intensity for infinite plate model.

Note S19. Comparison of the simulation design and results for finite plate models and infinite plate models.

The parameters utilized for the simulations are the same as those introduced in Note S9. For the infinite plate model, the infinite element domain is designed in the simulation, so the charge density is distributed on some infinite planes, and the electric field is uniform in both magnitude and direction, as shown in Fig. N20a. However, for the finite plate model, the infinite element domain is removed, and the length of the plates is set as 20 mm and the internal distance of the TENG model is set as 0.1 mm. In this case, the electric field distribution is shown in Fig. N20b, which is much different from the former. The electric field distribution for the internal space of the TENG is shown in Fig. N20c, demonstrating high similarity to that shown in Fig. 6b. This is due to its much larger size compared with the internal distance.

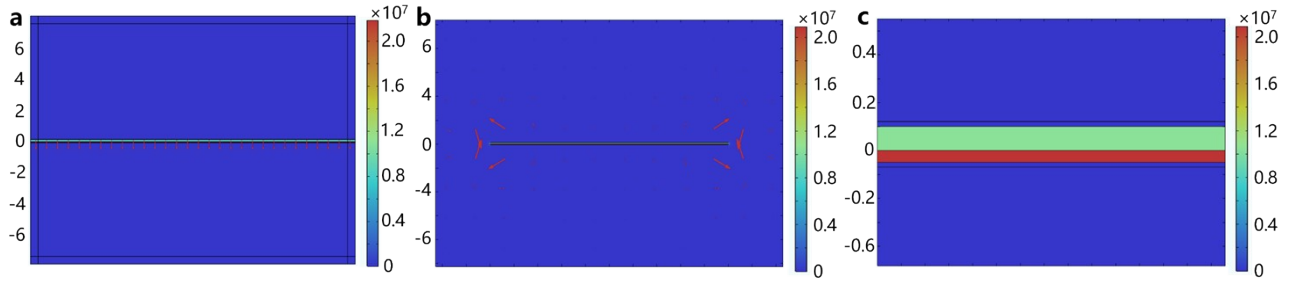

Fig. N20 Simulation for the finite and infinite plate models. Electric field distribution for **a** the infinite plate model, **b** the finite plate model and **c** internal space of the TENG in the finite plate model (nearly uniform).

Note S20. Simulation results of the infinite plate model with a larger internal distance.

For the infinite plate model, when the internal distance of the TENG increases, the distribution of the electric field remains uniform in magnitude and direction, as shown in Fig. N21a. Comparing Fig. N21b with Fig. 4e, it can be seen that the electric field intensity in each region remains unchanged with the increase of the internal distance. This is different for the results obtained from the finite plate model. And the electric field intensity inside the TENG, E_3, as shown in Fig. N21b is obviously larger than that shown in Fig. 7f.

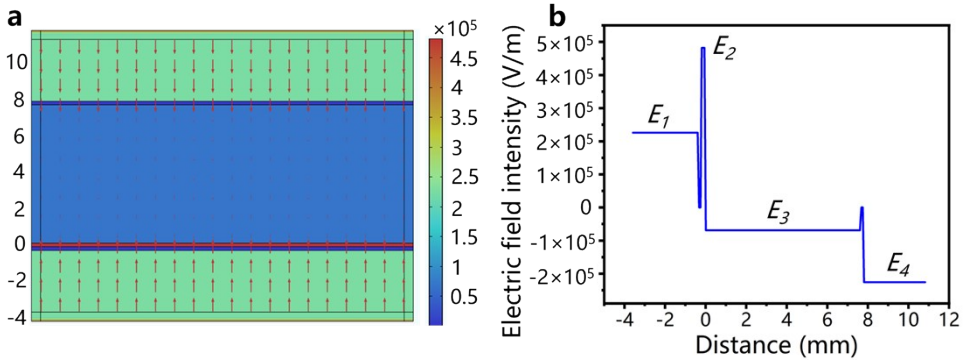

Fig. N21 Simulation of the infinite plate model with a larger internal distance. **a** Distribution of the electric field. **b** Variation of the electric field intensity with the distance.

Note S21. Explanation for the free charge redistribution.

Usually, the dielectric material tends to acquire electrons when in contact with the metal electrode. For metallic materials, free charges are all distributed on the surface. While when the dielectric material acquires electrons, they will diffuse into the material. The redistribution of free charges can occur on all materials. According to the current continuity equation and Gaussian electric field theorem:

$$\nabla \times \mathbf{J} + \frac{\partial \rho}{\partial t} = 0$$

$$\nabla \times \mathbf{E} = \frac{\rho}{\varepsilon}$$

The equation can be derived:

$$\frac{\partial \rho}{\partial t} + \frac{\sigma \rho}{\varepsilon} = 0$$

Its solution is

$$\rho(\mathbf{r}, t) = \rho(\mathbf{r}, 0) e^{-\frac{\sigma}{\varepsilon} t}$$

Where $\rho(\mathbf{r}, 0)$ is the initial value (t = 0) for the charge distribution, and the initial charge distribution at each point on the material decays exponentially with time t. And σ/ε is relaxation time, that is, the time required at any point for the charges reducing to 1/e of its original value. For metallic materials, the redistribution of charges will be completed in a very short time, while for dielectric materials, the process can be very slow. Therefore, when the dielectric material acquires additional surface charge through contact electrification, these charges will gradually diffuse into the material and form a distribution of bulk charge.

Note S22. Analysis for the ferroelectric material based TENG.

In this study, we analyze the TENG theory from initial charge distribution. We have triboelectric charges, pre-charging charges on the dielectric material, and compensation charge on the base electrode. From the eqn 30 in the manuscript we can see that the increase of triboelectric charges and pre-charging charges will increase the charge transfer of the TENG.

For the ferroelectric material, the reference[16] shows that the ferroelectric material can attract a significant amount of electrons from the opposite triboelectric material, and a high-performance TENG is fabricated based on the ferroelectric material. This means the triboelectric charges of the TENG can be increased due to the effect of the ferroelectric material. The internal electric field of the dielectric material is a kind of polarization electric field **P** caused by electric dipoles. If we have a macroscopically small and microscopically large volume in the ferroelectric material, then

$$\mathbf{P} = \lim_{\Delta V \to 0} \frac{\sum \mathbf{p}}{\Delta V} = \lim_{V \to 0} \frac{\sum q\mathbf{l}}{\Delta V}$$

Where p is electric dipole moment, V is the chosen volume, q is the charge for the dipole and **l** is the internal distance of the dipole with direction (point from negative charges to positive charges). If we know the electric field, we can calculate its equivalent bound charge inside the ferroelectric material:

$$\rho_b = \nabla \cdot \mathbf{P} = \frac{\partial P_x}{\partial x} + \frac{\partial P_y}{\partial y} + \frac{\partial P_z}{\partial z}$$

This is equivalent to the pre-charging charges (including surface charges and bulk charges), which plays an important role and can be used to enhance the output of the TENG. When we have the triboelectric charges and pre-charging charges, we can use the proposed models to analyze the TENG based on the ferroelectric material. Therefore, the theory proposed in this study can provide approaches for analyzing ferroelectric material based TENGs.

Note S23. Calculations for the potential in electrodynamic model.

The potential generated by the charges distributed on the independent electrode:

$$\varphi_m(\mathbf{r}) = \frac{1}{4\pi\varepsilon_0}\int_S \frac{\sigma'_{mu}(\mathbf{r}'_{\mathbf{mu}})}{|\mathbf{r}-\mathbf{r}'_{\mathbf{mu}}|}dS' + \frac{1}{4\pi\varepsilon_0}\int_S \frac{\sigma'_{mu}(\mathbf{r}'_{\mathbf{md}})}{|\mathbf{r}-\mathbf{r}'_{\mathbf{md}}|}dS'$$

The potential generated by the charges distributed on the dielectric material:

$$\varphi_d(\mathbf{r}) = \frac{1}{4\pi\varepsilon_0}\int_S \frac{\sigma_t(\mathbf{r}'_{\mathbf{t}})}{|\mathbf{r}-\mathbf{r}'_{\mathbf{t}}|}dS' + \frac{1}{4\pi\varepsilon_0}\int_V \frac{\rho_t(\mathbf{r}'_{\mathbf{t}})}{|\mathbf{r}-\mathbf{r}'_{\mathbf{t}}|}dV' + \frac{1}{4\pi\varepsilon_0}\oint_S \frac{\mathbf{P}(\mathbf{r}'_{\mathbf{p}})\cdot\mathbf{n}}{|\mathbf{r}-\mathbf{r}'_{\mathbf{t}}|}dS' + \frac{1}{4\pi\varepsilon_0}\int_V \frac{-\nabla\cdot\mathbf{P}(\mathbf{r}'_{\mathbf{p}})}{|\mathbf{r}-\mathbf{r}'_{\mathbf{t}}|}dV'$$

The potential generated by the charges distributed on the base electrode:

$$\varphi_e(\mathbf{r}) = \frac{1}{4\pi\varepsilon_0}\int_S \frac{\sigma'_{eu}(\mathbf{r}'_{\mathbf{eu}})}{|\mathbf{r}-\mathbf{r}'_{\mathbf{eu}}|}dS' + \frac{1}{4\pi\varepsilon_0}\int_S \frac{\sigma'_{ed}(\mathbf{r}'_{\mathbf{ed}})}{|\mathbf{r}-\mathbf{r}'_{\mathbf{eu}}|}dS'$$

Definition of the polarization electric field:

$$\mathbf{P} = \lim_{\Delta V\to 0}\frac{\sum \mathbf{p}}{\Delta V} = \lim_{V\to 0}\frac{\sum q\mathbf{l}}{\Delta V}$$

The total potential in space:

$$\varphi(\mathbf{r}) = \varphi_m(\mathbf{r}) + \varphi_d(\mathbf{r}) + \varphi_e(\mathbf{r})$$

Displacement current density in space:

$$\begin{aligned} J_d = \frac{\varepsilon_r}{4\pi}\partial\Big[&\int_S \frac{\sigma'_{mu}(\mathbf{r}'_{\mathbf{mu}})\cdot(\mathbf{r}_{\mathbf{mo}}-\mathbf{r}'_{\mathbf{mu}})}{|\mathbf{r}-\mathbf{r}'_{\mathbf{mu}}|^3}dS' + \int_S \frac{\sigma'_{mu}(\mathbf{r}'_{\mathbf{md}})\cdot(\mathbf{r}_{\mathbf{mo}}-\mathbf{r}'_{\mathbf{md}})}{|\mathbf{r}-\mathbf{r}'_{\mathbf{md}}|^3}dS' + \int_S \frac{\sigma_t(\mathbf{r}'_{\mathbf{t}})\cdot(\mathbf{r}_{\mathbf{mo}}-\mathbf{r}'_{\mathbf{t}})}{|\mathbf{r}-\mathbf{r}'_{\mathbf{t}}|^3}dS' \\ &+\int_V \frac{\rho_t(\mathbf{r}'_{\mathbf{t}})\cdot(\mathbf{r}_{\mathbf{mo}}-\mathbf{r}'_{\mathbf{t}})}{|\mathbf{r}-\mathbf{r}'_{\mathbf{t}}|^3}dV' + \oint_S \frac{\mathbf{P}(\mathbf{r}'_{\mathbf{p}})\cdot\mathbf{n}\cdot(\mathbf{r}_{\mathbf{mo}}-\mathbf{r}'_{\mathbf{p}})}{|\mathbf{r}-\mathbf{r}'_{\mathbf{p}}|^3}dS' + \int_V \frac{-\nabla\cdot\mathbf{P}(\mathbf{r}'_{\mathbf{p}})\cdot(\mathbf{r}_{\mathbf{mo}}-\mathbf{r}'_{\mathbf{p}})}{|\mathbf{r}-\mathbf{r}'_{\mathbf{p}}|^3}dV' \\ &+\int_S \frac{\sigma'_{eu}(\mathbf{r}'_{\mathbf{eu}})\cdot(\mathbf{r}_{\mathbf{mo}}-\mathbf{r}'_{\mathbf{eu}})}{|\mathbf{r}-\mathbf{r}'_{\mathbf{eu}}|^3}dS' + \int_S \frac{\sigma'_{ed}(\mathbf{r}'_{\mathbf{ed}})\cdot(\mathbf{r}_{\mathbf{mo}}-\mathbf{r}'_{\mathbf{ed}})}{|\mathbf{r}-\mathbf{r}'_{\mathbf{ed}}|^3}dS'\Big]/\partial t \end{aligned}$$

Note S24. Comparison between the original FEP film and the pre-charging FEP film.

We can pre-charging charges for the dielectric material by triboelectrification process. The comparison between the original FEP film and the pre-charging FEP film (with PET material) is shown in Fig. N22. Obviously, the pre-charging FEP film has a high surface potential, indicating that there have been more surface charges on the material. Atomic force microscopy (Cypher-ES) was used to scan the surface topography and surface potential of the FEP film, and the probe model is ASYELEC-01-R2 (1.42 nN nm−1).

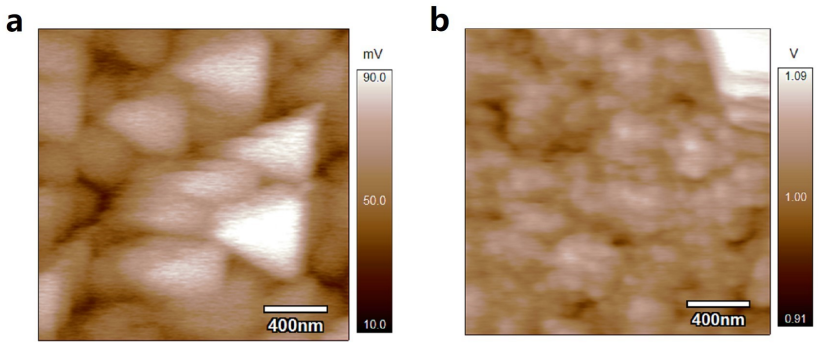

Fig. N22 Comparison between the original FEP film and the pre-charging FEP film. Surface potential of the **a** normal and **b** pre-charging FEP material.

Note S25. TENG-based communication method.

This method is from a reference[17]. As shown in Fig. N23, the TENG is in contact-separation motion by a linear motor. One electrode of the TENG is grounded and another electrode is connected to the transmitting electrode. The electric field in the space can be received by the receiving electrode, which is connected to the electrometer. The received voltage is shown in Fig. N23b-c.

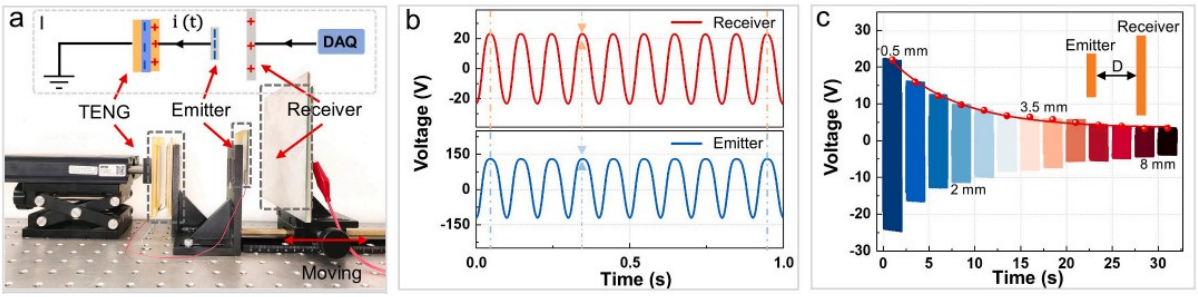

Fig. N23 a Experimental setup for transmission characteristics measurements. Inset is the diagram of equivalent circuit. **b** Information transmission between the emitter and the receiver at a distance of 0.5 mm. **c** Relative change in voltage of the receiver with different distances (from *Nano Energy, 2023, 118: 109001*).

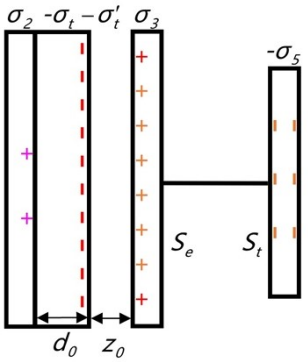

Fig. N24 The TENG model when the base electrode is not grounded.

The schematic diagram of the experiment is shown in Fig.N24. The TENG is composed of a FEP film with conductive ink electrode and an aluminum film. The TENG is fixed by wood substrates and in contact-separation motion controlled by a linear motor. The independent electrode is connected to the transmitting electrode. The distance between the transmitting electrode and receiving electrode is 15 cm. And the receiving electrode is connected to an electrometer to detect the electrical signal.

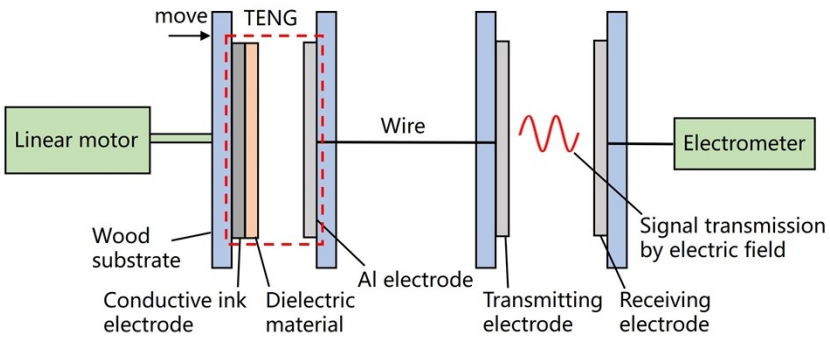

Fig. N25 Schematic diagram of the TENG-based communication experiment.

Supplementary References

1. S. Niu, S. Wang, L. Lin, Y. Liu, Y. S. Zhou, Y. Hu and Z. L. Wang, *Energy & Environmental Science*, 2013, **6**, 3576.
2. B. Yang, W. Zeng, Z. H. Peng, S. R. Liu, K. Chen and X. M. Tao, *Advanced Energy Materials*, 2016, **6**, 1600505.
3. R. D. I. G. Dharmasena, K. D. G. I. Jayawardena, C. A. Mills, J. H. B. Deane, J. V. Anguita, R. A. Dorey and S. R. P. Silva, *Energy & Environmental Science*, 2017, **10**, 1801-1811.
4. J. Shao, M. Willatzen, Y. Shi and Z. L. Wang, *Nano Energy*, 2019, **60**, 630-640.
5. X. Chen, F. Zhang, C. Han, Y. Liu, G. Y. Chen, X. Sun and Z. Wen, *Nano Energy*, 2023, **111**, 108435.
6. J. Shao, M. Willatzen and Z. L. Wang, *Journal of Applied Physics*, 2020, **128**, 111101.
7. A. A. Mathew and S. Vivekanandan, *Energy Technology*, 2022, **10**, 2101130.
8. W. Akram, Q. Chen, G. Xia and J. Fang, *Nano Energy*, 2023, **106**.
9. H. Ko, Y.-w. Lim, S. Han, C. K. Jeong and S. B. Cho, *ACS Energy Letters*, 2021, **6**, 2792-2799.
10. X. Xiao, X. Zhang, S. Wang, H. Ouyang, P. Chen, L. Song, H. Yuan, Y. Ji, P. Wang, Z. Li, M. Xu and Z. L. Wang, *Advanced Energy Materials*, 2019, **9**, 1902460.
11. M. Xu, P. Wang, Y.-C. Wang, S. L. Zhang, A. C. Wang, C. Zhang, Z. Wang, X. Pan and Z. L. Wang, *Adv. Energy Mater.*, 2018, **8**, 1702432.
12. Y. Lu, H. Tian, J. Cheng, F. Zhu, B. Liu, S. Wei, L. Ji and Z. L. Wang, *Nature Communications*, 2022, **13**, 108043.
13. M. Xu, T. Zhao, C. Wang, S. L. Zhang, Z. Li, X. Pan and Z. L. Wang, *ACS nano*, 2019, **13**, 1932-1939.
14. H. Zhao, X. Xiao, P. Xu, T. Zhao, L. Song, X. Pan, J. Mi, M. Xu and Z. L. Wang, *Advanced Energy Materials*, 2019, **9**, 1902824.
15. H. Zhao, M. Shu, Z. Ai, Z. Lou, K. W. Sou, C. Lu, Y. Jin, Z. Wang, J. Wang, C. Wu, Y. Cao, X. Xu and W. Ding, *Advanced Energy Materials*, 2022, **12**, 2270154.
16. W. Seung, H. J. Yoon, T. Y. Kim, H. Ryu, J. Kim, J. H. Lee, J. H. Lee, S. Kim, Y. K. Park, Y. J. Park and S. W. Kim, *Advanced Energy Materials*, 2016, **7**, 1600988.
17. L. Tang, X. Hui, J. Chen, H. Guo and F. Wu, *Nano Energy*, 2023, **118**, 109001.